

Reduced Order Models for conduction and radiation inside semi-transparent media via the Modal Identification Method

Manuel Girault, Yang Liu, Yann Billaud, Adel Benselama, Didier Saury, Denis Lemonnier

▶ **To cite this version:**

Manuel Girault, Yang Liu, Yann Billaud, Adel Benselama, Didier Saury, et al.. Reduced Order Models for conduction and radiation inside semi-transparent media via the Modal Identification Method. International Journal of Heat and Mass Transfer, 2021, 168, 10.1016/j.ijheatmasstransfer.2020.120598 . hal-03103622

HAL Id: hal-03103622
https://hal.science/hal-03103622

Submitted on 8 Jan 2021

HAL is a multi-disciplinary open access archive for the deposit and dissemination of scientific research documents, whether they are published or not. The documents may come from teaching and research institutions in France or abroad, or from public or private research centers.

L'archive ouverte pluridisciplinaire **HAL**, est destinée au dépôt et à la diffusion de documents scientifiques de niveau recherche, publiés ou non, émanant des établissements d'enseignement et de recherche français ou étrangers, des laboratoires publics ou privés.

Reduced Order Models for conduction and radiation inside semi-transparent media via the Modal Identification Method

Manuel GIRAULT[a]*, Yang LIU[a,b], Yann BILLAUD[a], Adel BENSELAMA[a],
Didier SAURY[a], Denis LEMONNIER[a]

[a] Institut PPRIME UPR CNRS 3346 - CNRS ⋄ ISAE-ENSMA ⋄ Université de Poitiers
ENSMA, Téléport 2, 1 avenue Clément ADER, BP 40109
F-86961 Futuroscope Chasseneuil CEDEX

[b] Sino-European Institute of Aviation Engineering (SIAE), Civil Aviation University of China (CAUC), Tianjin, China

* corresponding author: manuel.girault@ensma.fr

Abstract

In the frame of characterization of thermophysical properties of semi-transparent gray media for which radiative transfers can be modelled by P1 approximation, the present study deals with development, construction and validation of conducto-radiative linear reduced order models (ROMs) explicitly parametrized by thermal conductivity and effective absorption coefficient. As variations of temperature are assumed to be limited in magnitude (about a few tenths of K) in the considered applications, the radiative contribution is linearized in the ROM formulation. ROMs are built through the Modal Identification Method (MIM): once their general form has been derived, they are identified using Particle Swarm Optimization and Ordinary Least Squares, from simulations coming from a nonlinear reference model. In the presented application, the latter is a two-dimensional axisymmetric unsteady model designed to model a “flash-type” experiment. The chosen range of values for thermal conductivity and effective absorption coefficient includes the values usually found for polymethyl methacrylate (PMMA). In comparison with the reference model, the computing time is considerably reduced with limited loss of accuracy.

Keywords: conduction; radiation; semi-transparent medium; P1 approximation; low order model; particle swarm optimization.

1 Introduction

In most applications involving heat transfer across semi-transparent media, the knowledge of both conductive and radiative properties is of essential importance. In particular, this is the case for polymethyl methacrylate (PMMA), also known as acrylic glass or Plexiglas®. PMMA is a semi-transparent thermoplastic material often used as an alternative to glass due to its lightweight and its remarkable mechanical properties. PMMA is used in a wide range of fields and applications such as aircraft construction (thermal insulators in motors [1] or composite materials [2] for instance), building windows, lenses, photovoltaic cells and many other applications. Consequently, the determination of thermophysical properties of PMMA in coupled radiation and conduction problems is of prime importance, especially with regard to the radiation absorption which exhibits a complex behavior. Although PMMA is a non-gray

participating medium, i.e. its radiation absorption capability depends strongly on the wavelength, the effective absorption coefficient is considered in this work, instead. The effective absorption expresses the integrated intensity for a homogeneous and isothermal non gray medium. In this work a gray-medium transport equation is considered, which is an approximation commonly used to the integrated radiative intensity for medium with moderate temperature gradients. Despite that assumption, which reduces the number of radiative transfer equations to be solved from many (depending on the medium radiative model) to one (i.e. gray radiative model), the resolution of coupled conduction-radiation problems may lead to prohibitive computational time, especially when an iterative procedure is involved, which is usually the case. This observation is especially true when multidimensional effects cannot be ignored leading to large systems of nonlinear equations due to the spatial discretization of the domain. In this context, model reduction is useful as it allows reducing the size of the model, hereafter referred to as Detailed Model (DM), from the number of discretization nodes to a much smaller size by means of a Reduced Order Model (ROM). A ROM is a model with a small number of degrees of freedom (dof), able to mimic the behavior of an actual physical system or a reference model of that system. A ROM allows computing the system response (observable outputs of interest or even the whole field) whatever the applied inputs, i.e. time-varying boundary conditions and/or volumetric source terms, and/or a range of values of some parameters, with limited loss of accuracy and much smaller computing time. A ROM can be obtained by transformation of a DM or identified from data coming either from simulations of a DM or from measurements on the actual system.

Park et al. [3] used the Proper Orthogonal Decomposition (POD), also known as Karhunen-Loève (KL) decomposition, combined with a Galerkin projection, to build a ROM for heat transfer by conduction and radiation (absorption, emission and scattering) in a homogeneous, isotropic and gray medium. The problem was clearly nonlinear due to the large variations of temperature (several hundreds of K). A material is defined there through scattering albedo $\omega = \sigma/(\sigma + \kappa)$ and extinction coefficient $\beta = \sigma + \kappa$, where σ and κ are the scattering and absorption coefficients, respectively. Transient snapshots of the temperature and incident radiation fields as a response of a step of prescribed temperature (Dirichlet thermal boundary condition), were computed with a reference detailed model (finite difference for energy equation and S4 method for RTE) and used to build empirical eigenfunctions via POD. The POD-Galerkin ROM so obtained was tested with the same reference values of parameters, first with the same step signal and then with a sinusoidal temperature signal. Both tests were successful. Not surprisingly, this first ROM showed discrepancies with simulations from the reference model when tested with the same temperature step signal but with parameter values different of the reference values used for generating snapshots for POD. In order to include dynamics corresponding to other parameter values, a second ROM was built with snapshots associated with 5 couples of parameter values (reference couple and 4 additional couples of parameters). This second ROM was tested with these 5 couples of parameters and gave good agreement but the authors did not mention which temperature signal was used and it is legitimate to wonder if it were the step signal used for snapshots. In such case, a good behavior is unsurprisingly expected. In the end only the first ROM seems to have been tested with a temperature signal different from the one used to generate snapshots. For the second

ROM, test results for parameter couples different from the 5 couples used to generate the snapshots employed for the ROM construction were not presented in [3]. However, the second ROM appears to work well for other values of parameters as it was used by Park and Yoon [4] for solving an inverse problem for the estimation of the absorption coefficient κ and scattering coefficient σ from simulated temperature measurements with the conjugate gradient method. Although authors did not show the temperature signal used to simulate temperature measurements for the inverse problem, one can infer from the evolution of sensitivities of the temperature with respect to κ and σ as functions of time, that the temperature signal used to simulate temperatures for the inverse problem is the same as the one used to generate snapshots and hence build the ROM, which obviously makes the inverse problem much easier to solve with this ROM. In fact, in both [3] and [4], one may wonder how would behave the ROM built from 5 couples of parameter values and the step signal when used with other parameter values and a different prescribed temperature signal. In both papers the considered medium seems to be quite fictitious (density ρ = 0.4 kg.m^{-3}, specific heat capacity C_p = 1100 J.kg^{-1}.K^{-1} and thermal conductivity k_{th} = 44 W.m^{-1}.K^{-1}, thus resulting in thermal diffusivity α = 0.1 m^2.s^{-1}). In [5], Park and Sung also use a ROM based on POD to solve an inverse radiation problem for the estimation of a time-varying heat source in an enclosure with a participating medium (same as above).

The Amalgam Reduced Order Modal Model (AROMM) method is based on a special spectral problem where the eigenvalue of each mode appears in a Steklov boundary condition, thus allowing the handling of nonlinear problems. The amalgamation of the branch modes then allows obtaining a ROM from the reference large-size DM. Gaume et al. [6] recently applied this method on a furnace where a titanium object of complex shape is heated by radiant tubes. The enclosure is filled with a non-participating medium and radiation between heaters and object is modelled by radiosity method. The ROM allows computing the time-varying temperature distribution in the furnace and in particular in the heated object for different values of external heat exchange coefficient and temperature of radiant tubes.

In the field of electronics, Fagiano and Gati [7] developed an approach to build ROMs for thermal radiation from plasma arcs in switchgear devices. The heat radiation problem is first modelled as a Linear Parameter Varying (LPV) full order model with one input (black-body intensity), one output (radiation intensity), three parameters (temperature, pressure, gas composition), and a large number of internal states (one for each considered frequency of the electromagnetic spectrum. The LPV ROM has the same form as the LPV full order model but with only a few bands of frequencies. The ROM parameters, which in fact are used for parametrizing “equivalent” absorption coefficient and spectral emissivity functions, are identified through a nonlinear optimization problem.

To the best knowledge of the authors, other existing reduction methods have up to now not been applied to heat transfer problems involving radiation through participating media or between surfaces.

In the present work the Modal Identification Method (MIM) [8] [9] [10] [11] [12] [13] is used to build ROMs of heat transfer for coupled conduction and linearized radiation (by absorption and emission) in semi-transparent media. MIM shares common features with POD-Galerkin

but also has significant differences. In both approaches, as in many model reduction methods, each variable field (e.g. temperature, incident radiation, velocity, etc.) is written as a sum of products of space functions by time functions, in fact it is a linear combination of space functions with time-dependent coefficients. Moreover both methods use space and time data obtained either by numerical simulation issued from a reference detailed model (DM) sometimes called full order model, or by measurements recorded on the actual system (experimental set-up or industrial plant for instance). In the POD-Galerkin approach the ROM equations are obtained via a Galerkin projection of local governing equations and the components of the ROM constitutive elements are computed with the space functions issued from POD performed over data covering space and time [3]. In order to compute these space functions, it is required for data to cover the entire spatial domain or at least a part of it for which the ROM is built (a 2D plane in a 3D problem for instance). The MIM also requires the knowledge of the local governing equations. In the MIM approach, the ROM equations may also be written down using a Galerkin projection [10], [12] but only the form of these equations is important. The components of the ROM constitutive elements are not computed using their literal expressions like in POD-Galerkin, they are identified through a parameter estimation problem corresponding to the minimization of a quadratic functional based on the difference between reference output data, on the one hand, and on the ROM outputs corresponding to the same inputs, on the other hand [8]. Thus, MIM does not require data fields over the entire spatial domain. A ROM can be built for a restricted set of observables located at chosen locations (even a single observable as in the present paper). MIM does not also require to perform a POD on the data. In return of such benefits, the parameter estimation problem requires to use optimization techniques (Particle Swarm Optimization [14] and Ordinary Least Squares).

MIM was applied successfully on several heat transfer problems. Let us mention a few dealing with heat conduction. In [9], a transient inverse problem for the estimation of two time-varying internal heat sources from surface temperature measurements, on a system involving both radiative and convective boundary conditions, was fruitfully solved with ROMs identified by MIM from experimental data. ROMs having as input both a time-varying heat flux density and a physical parameter in a predefined range (thermal conductivity) were built in [10], where the inverse problem for the estimation of thermal conductivity from temperature data was also carried out with these ROMs. State-feedback control problems were also addressed. As an example, real time thermal regulation within 0.01°C of an ultra-high precision metrology system was successfully performed by model predictive control using in-situ built ROMs [11]. MIM has also been used to build ROMs for non-isothermal flows, for instance a 2D laminar mixed convection flow around a heated circular cylinder [12]. In the frame of characterization of melted polymer flows, a thermo-rheological ROM for a pseudo-plastic fluid flow in a circular runner, taking into account transport, conduction and heat dissipation due to viscous effects in high shear zones, was developed in [13]. The ROM, whose output was the temperature profile in the channel outlet section, was explicitly parametrized by two parameters: the consistency index and the flow behavior index defining a power-law model of dynamic viscosity.

It should be emphasized that POD-Galerkin may lead to unstable ROMs (in the sense of Lyapunov Stability), even for linear Partial Differential Equations as shown by Kalashnikova et al. [15]. These authors proposed to stabilize the ROMs issued from POD by using a constrained nonlinear least squares optimization problem over the unstable eigenvalues of the Linear Time Invariant ROM state matrix: the output error between the reference full order model and the ROM is minimized subject to the constraint that the real part of the eigenvalues must be strictly negative. This approach is in fact very close to the one used in MIM when building non-parametric linear ROMs, for linear heat conduction problems for instance [11]: the ROM being written under modal from, the components of the diagonal state matrix are identified through the nonlinear output error minimization problem subject to the constraint that they must be real strictly negative scalars, thus ensuring the ROM stability. In the present work, a particular care will be paid to the final parametric ROM equations whose specific form will ensure stability regardless the values of the parameters.

The present work is set in the frame of coupled heat transfers by conduction and radiation across gray semi-transparent media, such as glass and polymers, for which radiative transfers can be modelled suitably by P1 approximation [16]. Furthermore the temperature variations of limited range are assumed (about a few tenths of K), thus allowing linearization of the radiative contribution. The goal is to build linear ROMs having the ability to compute very quickly and with sufficient accuracy the evolution of temperature at locations of interest in response to unsteady boundary conditions, with thermal conductivity k_{th} and effective absorption coefficient κ of the medium as explicit parameters. Once the governing equations and general boundary conditions are presented in section 2, a brief overview of the MIM is given in section 3. The parametric ROM equations are then derived in section 4 and the method for building a series of ROMs of different sizes is described in section 5. In section 6, the proposed approach is then applied to a test problem for which the reference model is a two-dimensional axisymmetric unsteady model [17], [18] designed to mimic a “flash-type” experiment and based on the finite volumes method coupled with the P1 approximation. In this illustrative example, the ranges of k_{th} and κ values enclose the values found in the literature for PMMA. ROMs are tested with parameter values and applied heat flux signal both different from those used for the ROMs construction.

2 Local governing equations and boundary conditions

2.1 Local governing equations

Let us consider heat transfer by conduction and radiation within a gray, homogeneous, isotropic, absorbing, emitting and non-scattering medium with black boundary surfaces. Let us call Ω the domain and Γ its boundary. The problem may be either 1D, 2D or 3D.

The energy equation writes:

$$\rho C_p \frac{\partial T}{\partial t}(x,t) = -\vec{\nabla}.(\vec{q}_{cond} + \vec{q}_{rad}) \quad (1)$$

Where $x \in \Omega$ is the generic position in space and $t \in [0; t_f]$ is the time variable.

The conductive heat flux density vector $\vec{q}_{cond}$ is assumed to follow Fourier's law:

$$\vec{q}_{cond} = -k_{th}\vec{\nabla}T(x,t) \quad (2)$$

The radiative transfer equation (RTE) for a semi-transparent gray medium writes:

$$-\vec{\nabla}.\vec{q}_{rad} = \kappa(G(x,t) - 4\pi L^0(T)) \quad (3)$$

Where $\vec{q}_{rad}$ is the radiative heat flux density, κ the effective absorption coefficient, G the incident radiation and $L^0(T) = n^2\sigma T^4/\pi$ the total radiation intensity.

The P1 method [16], suitable for optically thick media, provides a relationship between the radiative heat flux density and the incident radiation:

$$\vec{q}_{rad} = -\frac{1}{3\kappa}\vec{\nabla}G(x,t) \quad (4)$$

Using (2) and (4), equations (1) and (3) can be written as:

$$\rho C_p \frac{\partial T}{\partial t}(x,t) = \vec{\nabla}.\left(k_{th}\vec{\nabla}T(x,t)\right) + \vec{\nabla}.\left(\frac{1}{3\kappa}\vec{\nabla}G(x,t)\right) \quad (5)$$

$$\vec{\nabla}.\left(\frac{1}{3\kappa}\vec{\nabla}G(x,t)\right) = \kappa(G(x,t) - 4n^2\sigma T^4(x,t)) \quad (6)$$

In equations (5) and (6), density ρ, specific heat capacity C_p, thermal conductivity k_{th}, effective absorption coefficient κ and refractive index n are considered uniform on domain Ω and independent of the temperature.

2.2 Boundary conditions

The thermal boundary condition is written in the following general form:

$$k_{th}\vec{\nabla}T.\vec{n} + \frac{1}{3\kappa}\vec{\nabla}G.\vec{n} = \gamma(x)\varphi(t) + h(x)\big(T_a - T(x,t)\big) \quad \forall x \in \Gamma, \forall t \in \left[0; t_f\right] \qquad (7)$$

Where $h(x)$ is the heat transfer coefficient distribution and T_a is the ambient temperature.

One may therefore define subparts of boundary Γ, each one with either a Fourier condition ($\gamma = 0$), a Neumann condition ($\gamma = 1$ and $h = 0$) or a mixed condition.

The radiative boundary condition is written according to Marshak's model [16], based on conservation of normal flux across the surface:

$$\frac{2}{3}\vec{\nabla}G.\vec{n} + \kappa G = 4\kappa n^2\sigma T^4 \quad \forall x \in \Gamma, \forall t \in \left[0; t_f\right] \qquad (8)$$

Assuming diffuse surfaces, the Marshak's model does not add any error to that of the P1 approximation itself.

The medium is considered to be initially at ambient temperature T_a ($T(t=0) = T_a$), thus corresponding to zero applied heat flux density ($\varphi(t=0) = 0$).

2.3 Linearization around nominal configuration

Let us consider a steady state corresponding to the temperature field $T_0(x)$ and incident radiation field $G_0(x)$ resulting from constant applied heat flux density φ_0. According to energy equation (5), RTE (6) and boundary conditions (7) and (8), these fields are solutions of:

$$0 = \vec{\nabla}.\left(k_{th}\vec{\nabla}T_0(x)\right) + \vec{\nabla}.\left(\frac{1}{3\kappa}\vec{\nabla}G_0(x)\right) \qquad (9)$$

And:

$$\vec{\nabla}.\left(\frac{1}{3\kappa}\vec{\nabla}G_0(x)\right) = \kappa\left(G_0(x) - 4n^2\sigma\big(T_0(x)\big)^4\right) \qquad (10)$$

With boundary conditions:

$$k_{th}\vec{\nabla}T_0(x).\vec{n} + \frac{1}{3\kappa}\vec{\nabla}G_0(x).\vec{n} = \gamma(x)\varphi_0 + h(x)\big(T_a - T_0(x)\big) \qquad (11)$$

And:

$$\frac{2}{3}\vec{\nabla}G_0(x).\vec{n} + \kappa G_0(x) = 4\kappa n^2\sigma\left(T_0(x)\right)^4 \quad (12)$$

Small heat flux density variation $\delta\varphi(t)$ and resulting small variations of temperature $\delta T(x,t)$ and incident radiation $\delta G(x,t)$ around this steady state are assumed. Heat flux density, temperature and incident radiation corresponding to these variations are written as:

$$\varphi(t) = \varphi_0 + \delta\varphi(t) \quad (13)$$

$$T(x,t) = T_0(x) + \delta T(x,t) \quad (14)$$

$$G(x,t) = G_0(x) + \delta G(x,t) \quad (15)$$

Injecting (14) and (15) in (5), then subtracting (9), we get the energy equation for δT and δG :

$$\rho C_p \frac{\partial \delta T}{\partial t}(x,t) = \vec{\nabla}.\left(k_{th}\vec{\nabla}\delta T(x,t)\right) + \vec{\nabla}.\left(\frac{1}{3\kappa}\vec{\nabla}\delta G(x,t)\right) \quad (16)$$

Injecting (14) and (15) in (6), developing the nonlinear term using the binomial theorem, then subtracting (10), we get the nonlinear RTE for δT and δG. Then, taking into account the assumption of small temperature variation δT, nonlinear terms i.e. terms in δT of degree higher than 1 are neglected, yielding the following linearized RTE for δT and δG:

$$\vec{\nabla}.\left(\frac{1}{3\kappa}\vec{\nabla}\delta G(x,t)\right) = \kappa\left(\delta G(x,t) - 16n^2\sigma\left(T_0(x)\right)^3\delta T(x,t)\right) \quad (17)$$

Such linearization can be justified even for $T_0 = 300\ K$ and temperature variations $\delta T(x,t)$ of about 30 K: for these values, comparing the two terms in δT and $(\delta T)^2$ in the expansion of $\left(T_0(x) + \delta T(x,t)\right)^4$ using the binomial theorem gives $4\left(T_0(x)\right)^3\delta T(x,t) = 3.24 \times 10^9\ K^4$ and $6\left(T_0(x)\right)^2\left(\delta T(x,t)\right)^2 = 4.86 \times 10^8\ K^4$.

Thermal and radiative boundary conditions for the linearized problem can be obtained in a similar manner from equations (7), (8), (11), (12), (13), (14) and (15):

$$k_{th}\vec{\nabla}\delta T(x,t).\vec{n} + \frac{1}{3\kappa}\vec{\nabla}\delta G(x,t).\vec{n} = \gamma(x)\delta\varphi(t) - h(x)\delta T(x,t) \quad (18)$$

$$\frac{2}{3}\vec{\nabla}\delta G(x,t).\vec{n} + \kappa\delta G(x,t) = 16\kappa n^2\sigma\left(T_0(x)\right)^3\delta T(x,t) \quad (19)$$

From now on, equations (16) to (19) will be considered for the ROM formulation. However, the numerical data from which the ROMs are going to be built will be simulated by a reference nonlinear DM.

The initial conditions for the linearized problem around nominal configuration are of course:

$$\delta T(x, t=0) = 0 \quad (20)$$

$$\delta G(x, t=0) = 0 \quad (21)$$

Corresponding to $\delta\varphi(t=0) = 0$.

The nominal steady state may be chosen so that the medium is at ambient temperature T_a : one has thus $\varphi_0 = 0$, $T_0(x) = T_a$ and $G_0(x) = 4n^2\sigma\left(T_0(x)\right)^4$.

3 Modal Identification Method: overview

We aim at building a ROM able to compute temperature values at some specific locations inside the domain and/or on its boundaries whatever the applied heat flux density signal $\delta\varphi(t)$ and whatever the values of thermal conductivity k_{th} and effective absorption coefficient κ in predefined ranges.

The approach used in the present paper is the Modal Identification Method (MIM) [8] [9] [10] [11] [12] [13]. The MIM consists of three main steps:

1) Defining the structure of the ROM equations able to adequately describe the involved physics (see section 4);
2) Generating some input-output data representative of the system. Those data may come from in-situ measurements or, as in the present work, from numerical simulations (see section 5.1 for a brief presentation and section 6.2 for the practical application);
3) Identifying the fixed constitutive parameters of the ROM equations through the minimization of a functional based on the quadratic residuals between the previously generated output data of the system, on the one hand, and the outputs of the ROM, on the other hand, for the same input data (see section 5.2 for a description of technical aspects and section 6.2 for results on the presented application).

The MIM therefore aims to adjust the ROM constitutive parameters using optimization techniques, in order for the ROM to mimic the data characterizing the input-output responses of the system.

4 Reduced Order Model formulation

4.1 Approximation of temperature and incident radiation

Fields of temperature variation $\delta T(x,t)$ and incident radiation variation $\delta G(x,t)$ are approximated as sums of products of space-varying functions and time-varying functions. This will allow us to separate space and time in the ROM. Let us write:

$$\delta T(x,t) \approx \sum_{i=1}^{m_T} \phi_i^{(T)}(x) a_i^{(T)}(t) \tag{22}$$

$\phi_i^{(T)}(x), i \in \{1, \dots, m_T\}$, are a truncation of an orthonormal basis of the Hilbert space formed by the space $\mathcal{L}_2(\Omega)$ of square integrable functions on Ω equipped with the usual inner product $\langle .,. \rangle$:

$$\langle u, v \rangle = \int_\Omega uv d\Omega \tag{23}$$

Orthonormality of functions $\phi_i^{(T)}(x), i \in \{1, \dots, m_T\}$ corresponds to the following property:

$$\langle \phi_i^{(T)}(x), \phi_j^{(T)}(x) \rangle = \int_\Omega \phi_i^{(T)}(x) \phi_j^{(T)}(x) d\Omega = \delta_{ij} \quad \forall i \in [1; m_T], \forall j \in [1; m_T] \tag{24}$$

Let us also write:

$$\delta G(x,t) \approx \sum_{i=1}^{m_G} \phi_i^{(G)}(x) a_i^{(G)}(t) \tag{25}$$

Where $\phi_i^{(G)}(x), i \in \{1, \dots, m_G\}$, are a truncation of another orthonormal basis of the same space. One therefore has:

$$\langle \phi_i^{(G)}(x), \phi_j^{(G)}(x) \rangle = \int_\Omega \phi_i^{(G)}(x) \phi_j^{(G)}(x) d\Omega = \delta_{ij} \quad \forall i \in [1; m_G], \forall j \in [1; m_G] \qquad (26)$$

At this point, we only seek to obtain the form of our ROM but at the time of the ROM identification, m_T and m_G will, of course, remain small.

4.2 Galerkin projections of energy and radiative transfer equations

The ROM formulation is obtained by writing down Galerkin projections of local conservation equations. For the sake of brevity, a short description of Galerkin projections of energy equation (16) and linearized radiative transfer equation (17), along with the introduction of boundary conditions (18) and (19), is given in section 1 of the appendix.

Coupled equations (A.5) and (A.13) (equations in the appendix are noted with an « A ») in matrix-vector form are obtained and written hereafter:

$$\frac{da^{(T)}(t)}{dt} = (k_{th} M_{Td} + M_{Th}) a^{(T)}(t) + \frac{1}{\kappa} M_{TG} a^{(G)}(t) + V \delta\varphi(t)$$

$$\left(\frac{1}{\kappa} M_{G0} + \kappa I_{m_G} + M_{G2}\right) a^{(G)}(t) = (\kappa M_{GT1} + M_{GT2}) a^{(T)}(t)$$

The involved matrices and vectors are defined in the appendix by equations (A.6) to (A.9) and (A.14) to (A.17). If space functions $\phi_k^{(T)}, k \in [1; m_T]$ and $\phi_k^{(G)}, k \in [1; m_G]$ were computed through Proper Orthogonal Decomposition (POD) of some temperature and incident radiation data, it would be possible to compute the elements defined in (A.6) to (A.9) and (A.14) to (A.17). Coupled equations (A.4) and (A.12) would thus form the so-called "POD-Galerkin" ROM. However, in the frame of the Modal Identification Method (MIM) used in this paper, space functions are not obtained via POD. The literal form of elements defined in (A.6) to (A.9) and (A.14) to (A.17) is not even taken into account. An optimization algorithm is used instead to build the ROM (see section 5.2). In order to reduce as much as possible the number of parameters to identify in the ROM construction, further processing is performed in the following section 4.3.

It is worth noticing that the case of several independent applied heat flux densities in the ROM formulation can be easily handled. Such case would correspond to have $\sum_{i=1}^{p} \gamma_i(x) \delta\varphi_i(t)$ instead of $\gamma(x)\delta\varphi(t)$ in thermal boundary condition (18), resulting in a $\sum_{i=1}^{p} V_i \delta\varphi_i(t)$ term in equation (A.5). However, building such a ROM via an identification procedure requires heat flux signals and resulting temperature data representative of the system behavior.

4.3 ROM in modal form: change of variables

Matrix M_{Td} defined by eq.(A.6) is symmetric. It is hence diagonalizable with real eigenvalues and its eigenvectors form an orthonormal basis of $\mathbb{R}^{m_T}$. Let us call D_T the diagonal matrix whose components are eigenvalues of M_{Td} and P_T the orthogonal matrix ($[P_T]^{-1} = [P_T]^T$) whose columns form a set of eigenvectors of M_{Td}.

One therefore has:

$$D_T = [P_T]^T M_{Td} P_T \tag{27}$$

Matrix M_{G0} defined by eq.(A.14) is also symmetric. Let us call D_G the diagonal matrix whose components are eigenvalues of M_{G0} and P_G the orthogonal matrix ($[P_G]^{-1} = [P_G]^T$) whose columns form a set of eigenvectors of M_{G0}.

One therefore has:

$$D_G = [P_G]^T M_{G0} P_G \tag{28}$$

The following changes of variables are now considered:

$$a^{(T)}(t) = P_T X^{(T)}(t) \tag{29}$$

$$a^{(G)}(t) = P_G X^{(G)}(t) \tag{30}$$

Let us now define the following matrices and vectors:

$$S_T = [P_T]^T M_{th} P_T, \quad A_{TG} = [P_T]^T M_{TG} P_G, \quad B = [P_T]^T V \tag{31}$$

Injecting changes of variables (29) and (30) into ROM for energy equation (A.5), performing the matrix-vector product of $[P_T]^{-1}$ ($= [P_T]^T$) with each term of the equation and taking equation (27) and notations (31) into account, one obtains the ROM for energy in modal form:

$$\frac{dX^{(T)}(t)}{dt} = (k_{th} D_T + S_T) X^{(T)}(t) + \frac{1}{\kappa} A_{TG} X^{(G)}(t) + B\delta\varphi(t) \tag{32}$$

Let us also define the following matrices:

$$S_G = [P_G]^T M_{G2} P_G, \quad A_{GT1} = [P_G]^T M_{GT1} P_T, \quad A_{GT2} = [P_G]^T M_{GT2} P_T \tag{33}$$

Injecting changes of variables (29) and (30) into ROM for RTE (A.13), performing the matrix-vector product of $[P_G]^{-1}$ $(= [P_G]^T)$ with each term of the equation and taking equation (28) and notations (33) into account, one obtains the ROM for RTE in modal form:

$$\left(\frac{1}{\kappa} D_G + \kappa I_{m_G} + S_G\right) X^{(G)}(t) = (\kappa A_{GT1} + A_{GT2}) X^{(T)}(t) \tag{34}$$

4.4 Particular form to ensure ROM stability

In order to ensure stability of the linear ROM for any choice of the values of parameters k_{th} and κ, the following constraints are enforced on constitutive matrices of equations (32) and (34):

i. Diagonal matrix D_T has negative components (possibly zero for some);
ii. $S_T = -[U_T]^T U_T$ with U_T an upper triangular matrix (possibly with some components of its diagonal equal to zero);
iii. Diagonal matrix D_G has positive components (possibly zero for some);
iv. $S_G = [U_G]^T U_G$ with U_G an upper triangular matrix (possibly with some components of its diagonal equal to zero);
v. $A_{GT1} = A_{GT2} = -[A_{TG}]^T$. One should note that even if the components of these matrices are equal, their dimensional units are not the same;
vi. Matrix A_{TG} is orthogonal i.e. $[A_{TG}]^{-1} = [A_{TG}]^T$. This requires the next condition;
vii. Matrix A_{TG} is a square matrix, i.e. $m_T = m_G = m$. In practice this is actually the case, independently of stability issues.

Taking constraint iv into account, let be the matrix A_G defined as:

$$A_G = \frac{1}{\kappa} D_G + \kappa I_{m_G} + \underbrace{[U_G]^T U_G}_{=S_G} \tag{35}$$

κ being strictly positive, constraint iii ensures that $\frac{1}{\kappa} D_G$ is symmetric semi-definite positive.

Matrix κI_{m_G} is also symmetric definite positive.

According to (33), matrix S_G is symmetric. Constraint iv is the Cholesky factorization of S_G and thus ensures that S_G is symmetric semi-definite positive.

Hence matrix A_G is the sum of three symmetric positive matrices, one being definite. A_G is therefore symmetric definite positive. So, A_G is invertible and its inverse $[A_G]^{-1}$ is also symmetric definite positive.

Hence, according to equations (34) and (35), one has:

$$X^{(G)}(t) = [A_G]^{-1}(\kappa A_{GT1} + A_{GT2}) X^{(T)}(t)$$

Which, thanks to constraint v, writes:

$$X^{(G)}(t) = -(\kappa + 1)[A_G]^{-1}[A_{TG}]^T X^{(T)}(t)$$

Injecting this expression into equation (32) and taking into account constraint ii leads to:

$$\frac{dX^{(T)}(t)}{dt} = \left(k_{th} D_T \underbrace{-[U_T]^T U_T}_{=S_T} - \left(1 + \frac{1}{\kappa}\right) A_{TG}[A_G]^{-1}[A_{TG}]^T \right) X^{(T)}(t) + B\delta\varphi(t) \quad (36)$$

Let us define matrix A_T as:

$$A_T = k_{th} D_T + S_T - \left(1 + \frac{1}{\kappa}\right) A_{TG}[A_G]^{-1}[A_{TG}]^T \quad (37)$$

Let us also define matrix S_{TG} as:

$$S_{TG} = A_{TG}[A_G]^{-1}[A_{TG}]^T \quad (38)$$

Obviously, S_{TG} is symmetric.

According to equation (38), matrix A_T defined by equation (37) also writes:

$$A_T = k_{th} D_T + S_T - \left(1 + \frac{1}{\kappa}\right) S_{TG}$$

k_{th} being strictly positive, constraint i ensures that $k_{th} D_T$ is symmetric semi-definite negative.

According to (31), matrix S_T is symmetric. Constraint ii is the Cholesky factorization of $-S_T$ and thus ensures that S_T is symmetric semi-definite negative.

$[A_G]^{-1}$ being symmetric definite positive, it can be diagonalized and thus written as $[A_G]^{-1} = PDP^T$ where D is diagonal with strictly positive components and P is orthogonal. Matrix S_{TG} defined by equation (38) therefore writes:

$$S_{TG} = A_{TG} PDP^T [A_{TG}]^T = A_{TG} PD[A_{TG} P]^T$$

Constraint vi states that A_{TG} is orthogonal. $A_{TG} P$ is thus the product of two orthogonal matrices and hence is also orthogonal. As a consequence, matrix S_{TG} is symmetric definite positive. κ being strictly positive, $-\left(1 + \frac{1}{\kappa}\right) S_{TG}$ is therefore symmetric definite negative.

Finally, matrix A_T is the sum of three symmetric negative matrices, one being definite. Subsequently, A_T is itself symmetric definite negative.

The dynamic system (36), which also writes $\frac{dX^{(T)}(t)}{dt} = A_T X^{(T)}(t) + B\delta\varphi(t)$ according to (37), is therefore stable (Lyapunov stability) regardless the values of k_{th} and κ.

Note that according to definition of A_{TG} in (31) and of A_{GT1} and A_{GT2} in (33), constraint v is equivalent to enforce $M_{GT1} = M_{GT2} = -[M_{TG}]^T$. Taking into account expressions of M_{TG}

(eq.(A.8)), M_{GT1} (eq.(A.16)) and M_{GT2} (eq.(A.17)), such a constraint corresponds to enforcing particular relationships between space functions $\phi_k^{(T)}$ and $\phi_k^{(G)}$, $\forall k \in [1; m]$.

4.5 Specific observables: output equation

We are interested in some observable temperatures at specific locations x_j, $j \in [1; N_{obs}]$ gathered in vector $\delta T_{obs} \in \mathbb{R}^{N_{obs}}$. According to the temperature field approximation (22) and defining matrix $C_{obs} \in \mathbb{R}^{N_{obs} \times m_T}$ such as $C_{ji} = \phi_i^{(T)}(x_j)$ $\forall j \in [1; N_{obs}], \forall i \in [1; m_T]$, one has:

$$[\delta T_{obs}]_j(t) = \delta T(x_j, t) = \sum_{i=1}^{m_T} \phi_i^{(T)}(x_j) a_i^{(T)}(t) = \sum_{i=1}^{m_T} (C_{obs})_{ji} a_i^{(T)}(t) \quad j \in [1; N_{obs}]$$

Which also writes in matrix form:

$$\delta T_{obs}(t) = C_{obs} a^{(T)}(t)$$

Injecting (29) in the above equation and defining $H = C_{obs} P_T \in \mathbb{R}^{N_{obs} \times m_T}$ leads to:

$$\delta T_{obs}(t) = H X^{(T)}(t) \tag{39}$$

Other observable quantities can be defined as linear combinations of such primary observables (average temperature on some chosen area, for instance).

4.6 Parametric ROM: summary

The parametric ROM is composed of:

- The dynamic system of equations (36), taking constraints i to vii of section 4.4 into account in order to ensure stability whatever the values of k_{th} and κ:

$$\frac{dX^{(T)}(t)}{dt} = \left(k_{th} D_T - [U_T]^T U_T - \left(1 + \frac{1}{\kappa}\right) A_{TG} [A_G]^{-1} [A_{TG}]^T\right) X^{(T)}(t) + B \delta\varphi(t)$$

  where D_T is diagonal with negative components, U_T is upper triangular, A_{TG} is orthogonal and A_G is defined by equation (35):

$$A_G = \frac{1}{\kappa} D_G + \kappa I_{m_G} + [U_G]^T U_G$$

where D_G is diagonal with positive components and U_G is upper triangular.

Equation (36), with A_G given by (35), allows computing the low-size vector $X^{(T)}(t) \in \mathbb{R}^m$ as a function of heat flux variation $\delta\varphi(t)$ and explicit parameters k_{th} and κ.

- The output equation (39) for computing the observable temperature vector $\delta T_{obs} \in \mathbb{R}^{N_{obs}}$ from $X^{(T)}(t) \in \mathbb{R}^m$:

$$\delta T_{obs}(t) = H X^{(T)}(t)$$

The initial thermal condition (20) of the linearized continuous problem implies $\delta T_{obs}(t=0) = 0$ and hence $X^{(T)}(t=0) = 0$ according to equation (39). Equation (36) in initial steady state is satisfied for $X^{(T)}(t=0) = 0$ and $\delta\varphi(t=0) = 0$.

5 Data generation and ROMs identification

Vector functions $X^{(T)}(t)$ and $\delta T_{obs}(t)$ depend on parameters k_{th} and κ. In the ROM identification process, notations $X^{(T)}(j,t)$ and $\delta T_{obs}(j,t)$ correspond respectively to the vector functions $X^{(T)}(t)$ and $\delta T_{obs}(t)$ associated with a particular couple $(k_{th},\kappa)_j$.

5.1 Data generation

The identification of the ROM constitutive parameters requires some input-output data:

- a chosen heat flux signal $\delta\varphi^{data}(t)$, corresponding in practice to discrete values $\delta\varphi^{data}(t_k), k \in [1; N_t^{id}]$, as well as a set of couples $(k_{th},\kappa)_j^{data}, j \in [1; N_c^{id}]$;
- the resulting observable temperatures $[\delta T_{obs}^{data}]_i(j,t_k),\ i \in [1; N_{obs}], j \in [1; N_c^{id}], k \in [1; N_t^{id}]$. In the present work, temperature data are computed with the Finite Volumes detailed model briefly presented in section 6.1.

It is worth noticing that although the ROM general form is independent of geometry and parameters ρ, C_p, n, the temperature data resulting from different geometries and/or different values of ρ, C_p, n, would, of course, lead to different ROMs.

5.2 ROMs identification

5.2.1 Optimization problem for the order m ROM

In order to effectively build a ROM of order m, elements of its constitutive matrices and vectors need to be computed. In the framework of the Modal Identification Method, rather

than taking their analytic form into account, their elements are identified through an algorithm using optimization techniques. The ROM construction is therefore recast into a parameter estimation problem. Parameters to be identified are components of:

- $D_T \in \mathbb{R}^{m\times m}$ diagonal, $U_T \in \mathbb{R}^{m\times m}$ upper triangular, $A_{TG} \in \mathbb{R}^{m\times m}$ orthogonal, $B \in \mathbb{R}^m$, $D_G \in \mathbb{R}^{m\times m}$ diagonal and $U_G \in \mathbb{R}^{m\times m}$ upper triangular in equations (35) and (36);
- $H \in \mathbb{R}^{N_{obs}\times m}$ in output equation (39).

For a given order m, the number of unknown parameters is hence:

$$N_{param}(m) = 2m^2 + 4m + N_{obs}m$$

Except for elements of matrix H whose identification is processed differently, unknown parameters to be identified are gathered into vector θ of size $N_\theta(m) = 2m^2 + 4m$.

All parameters are identified through the minimization of a functional $\mathcal{J}_{id}^{(m)}(\theta, H)$ based on the quadratic deviation between:

- the temperature $[\delta T_{obs}]$ computed with the ROM on the one hand (hence depending on θ and H), and
- the corresponding temperature data $\left[\delta T_{obs}^{data}\right]$, computed here with the reference detailed model (DM) on the other hand,

for the same applied heat flux signal $\delta\varphi^{data}(t_k), k \in \left[1; N_t^{id}\right]$ and the same set of couples $(k_{th}, \kappa)_j^{data}, j \in \left[1; N_c^{id}\right]$.

For a given order m, the quadratic functional $\mathcal{J}_{id}^{(m)}(\theta, H)$ therefore writes:

$$\mathcal{J}_{id}^{(m)}(\theta, H) = \sum_{i=1}^{N_{obs}} \sum_{j=1}^{N_c^{id}} \sum_{k=1}^{N_t^{id}} \left([\delta T_{obs}]_i(j, t_k, \theta, H) - \left[\delta T_{obs}^{data}\right]_i(j, t_k) \right)^2 \qquad (40)$$

In order to assess the quality of the identified ROM, the mean quadratic discrepancy $\sigma_{id}^{(m)}$ between data from DM and corresponding values computed by ROM is computed:

$$\sigma_{id}^{(m)} = \sqrt{\frac{\mathcal{J}_{id}^{(m)}(\theta, H)}{N_{obs} N_c^{id} N_t^{id}}} \qquad (41)$$

5.2.2 Identification procedure for ROM of order m

Equations (35), (36) and (39) show that ROM outputs δT_{obs} have nonlinear dependency on $D_T, U_T, A_{TG}, B, D_G, U_G$ and hence on θ, whereas they depend linearly on H. As a consequence, two types of optimization methods are used for the minimization of $\mathcal{J}_{id}^{(m)}(\theta, H)$ through a two-step approach. Both optimization algorithms are briefly described in section 2 of the appendix. A nonlinear iterative method is employed for the estimation of vector θ. A Particle Swarm Optimization (PSO) algorithm [14] has been used in the present work (cf. section 2.1

of appendix). At each iteration of the PSO algorithm, matrix H is computed via Ordinary Least Squares (cf. section 2.2 of appendix).

Figure 1 gives the identification procedure for a ROM of given order m in the Modal Identification Method. The stopping criterion is usually based on the fact that $\sigma_{id}^{(m)}$ does not decrease for a large number of successive iterations.

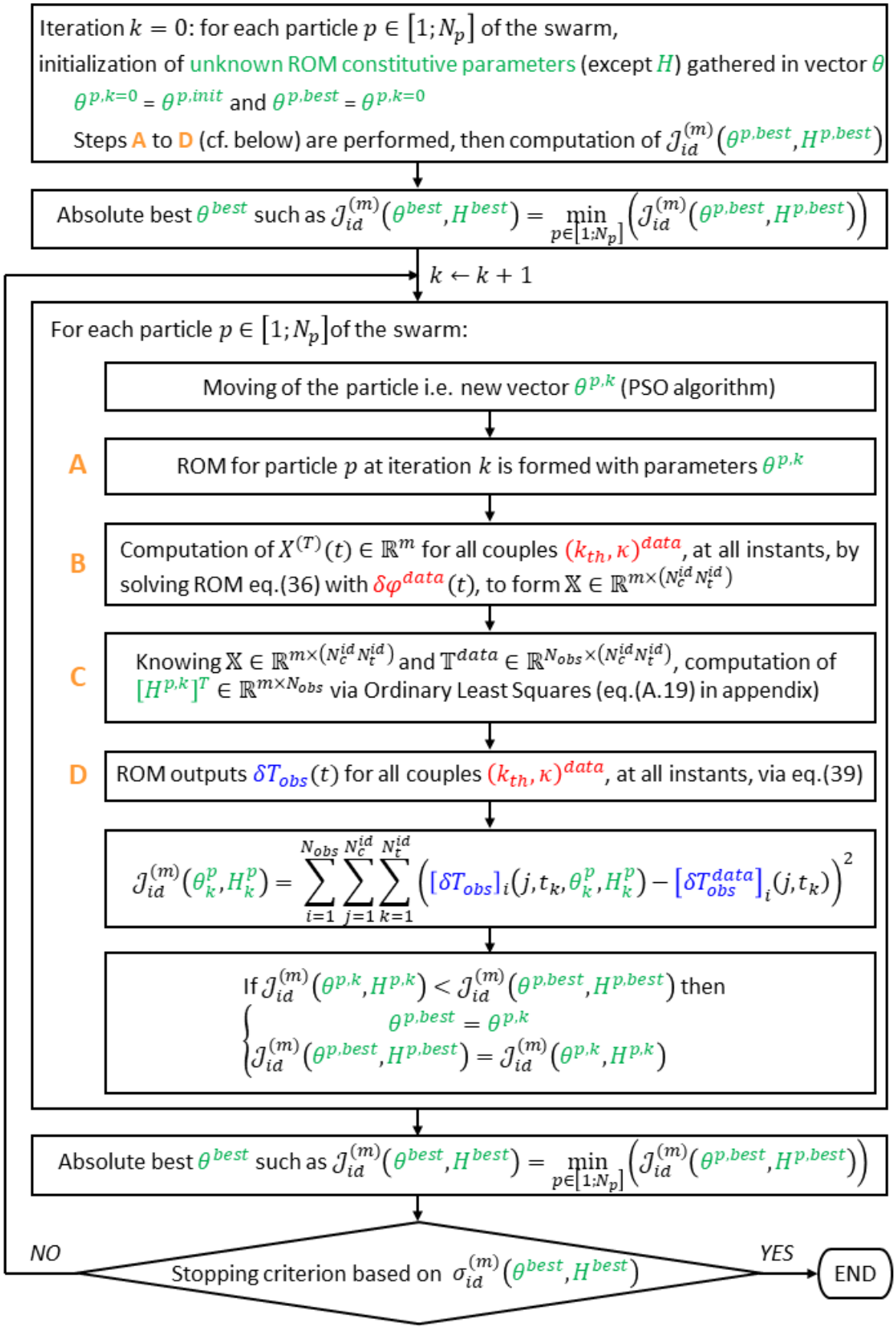


Figure 1. Summary of the identification procedure for a ROM of given order m

5.2.3 The global procedure for building a series of ROMs of successive orders

First of all $\mathcal{J}_{id}^{(1)}(\theta, H)$ is minimized in order to obtain θ and H associated with a single term in approximation of variables (equation (22) for temperature and equation (25) for incident radiation) and thus defining a ROM of order $m = 1$. A ROM of order $m = 2$ is then built by minimizing $\mathcal{J}_{id}^{(2)}(\theta, H)$ which leads to larger θ and H associated with two terms in approximation of variables. ROMs of higher order are then built by incrementing order m and minimizing corresponding functional $\mathcal{J}_{id}^{(m)}(\theta, H)$ until a predefined stopping criterion is satisfied. The global procedure is summarized as follows:

1. $m \leftarrow 1$
2. Minimization of $\mathcal{J}_{id}^{(1)}(\theta, H)$: identification of θ, H for order 1 ROM
3. $m \leftarrow m + 1$
4. Minimization of $\mathcal{J}_{id}^{(m+1)}(\theta, H)$: identification of new θ, H for order $m + 1$ ROM
5. Test of stopping criterion: 2 possibilities:
   - 5.1 if $\sigma_{id}^{(m+1)} \approx \sigma_{id}^{(m)}$ then STOP else go to 3
   - 5.2 if $\sigma_{id}^{(m)}$ reaches the wished accuracy, then STOP else go to 3

As vector θ is estimated via an iterative method (here PSO), an initial guess for θ is required.

As matrix H is computed by Ordinary Least Squares at each iteration of the PSO algorithm, no initial guess is needed for H.

For m=1, $D_T, U_T, A_{TG}, B, D_G, U_G$ come down to simple scalars, the ROM is thus defined by only 6 parameters. Only 5 of them are unknown as orthogonal matrix A_{TG} is equal to 1. They are randomly initialized with respect to constraints applied in section 4.4.

When identifying the order $m + 1$ ROM ($m \geq 1$), the parameters of the order m ROM previously identified are used as an initial guess for the corresponding unknown parameters in the order $m + 1$ ROM. In order to ensure this initial $m + 1$ ROM gives the same solutions as the order m ROM, the other parameters are initially set to zero, except for matrix A_{TG} for which $[A_{TG}]_{m+1,m+1}^{init} = 1$ in order to guarantee that A_{TG} in the order $m + 1$ ROM is initially orthogonal.

For initializing the identification of the order $m + 1$ ROM, we therefore set:

$$[D_T]^{init} = \begin{bmatrix} \overbrace{\begin{bmatrix} [D_T]_1 & 0 & \cdots & 0 \\ 0 & \ddots & \ddots & \vdots \\ \vdots & \ddots & \ddots & 0 \\ 0 & \cdots & 0 & [D_T]_m \end{bmatrix}}^{[D_T]^{order\ m\ ROM}} & \begin{matrix} 0 \\ \vdots \\ \vdots \\ 0 \end{matrix} \\ \begin{matrix} 0 & \cdots\cdots & \cdots\cdots & 0 \end{matrix} & 0 \end{bmatrix} \quad \text{and} \quad [U_T]^{init} = \begin{bmatrix} \overbrace{\begin{bmatrix} [U_T]_{11} & \cdots & \cdots & [U_T]_{1m} \\ 0 & \ddots & \ddots & \vdots \\ \vdots & \ddots & \ddots & \vdots \\ 0 & \cdots & 0 & [U_T]_{mm} \end{bmatrix}}^{[U_T]^{order\ m\ ROM}} & \begin{matrix} 0 \\ \vdots \\ \vdots \\ 0 \end{matrix} \\ \begin{matrix} 0 & \cdots\cdots & \cdots\cdots & 0 \end{matrix} & 0 \end{bmatrix}$$

Initialization of $[D_T]^{init}$ and $[U_T]^{init}$ is processed in a similar way.

Initially, matrices D_T, U_T, D_G, U_G are hence only semi-definite.

We also set:

$$[A_{TG}]^{init} = \begin{bmatrix} \underbrace{\begin{bmatrix} [A_{TG}]_{11} & \cdots & \cdots & [A_{TG}]_{1m} \\ \vdots & \ddots & \ddots & \vdots \\ \vdots & \ddots & \ddots & \vdots \\ [A_{TG}]_{m1} & \cdots & \cdots & [A_{TG}]_{mm} \end{bmatrix}}_{[A_{TG}]^{order\ m\ ROM}} & \begin{matrix} 0 \\ \vdots \\ \vdots \\ 0 \end{matrix} \\ \begin{matrix} 0 & \cdots\cdots & \cdots\cdots & 0 \end{matrix} & 1 \end{bmatrix} \quad \text{and} \quad [B]^{init} = \begin{bmatrix} \underbrace{\begin{bmatrix} B_1 \\ \vdots \\ B_m \end{bmatrix}}_{[B]^{order\ m\ ROM}} \\ 0 \end{bmatrix}$$

The functional $\mathcal{J}_{id}^{(m+1)}(\theta, H)$ to be minimized hence starts from the value obtained for $\mathcal{J}_{id}^{(m)}(\theta, H)$ and then decreases throughout iterations.

The series of ROMs of order 1 to m_{max} (m_{max} depending on the stopping criterion) is therefore built recursively, the ROM of order $m \geq 1$ being used to start the identification of the ROM of order $m+1$. The ROM of order m is neither a truncation of the ROM of order $m+1$ nor a truncation of the ROM of order m_{max}.

6 Application: heat flux on cylindrical STM sample

6.1 The considered configuration and the reference model

We consider a cylinder of diameter R and width e with black boundary surfaces, initially at thermal equilibrium with the environment ($T_0 = T_a = 300\ K$). The sizes are given in Figure 2. The heat exchange coefficient is $h = 5\ W.m^{-2}.K^{-1}$. Starting from $t = 0$, a time-varying localized heat flux density $\varphi(t)$ is imposed on the front face ($z = 0$), between $r = 0$ and $r = R_{\varphi(t)}$. Heat transfer within the medium is assumed to be two-dimensional axisymmetric. As the medium is assumed to be optically thick, the P1 method can be used and the present physical problem is described accurately by equations (5) and (6).

Boundary conditions are given as follows, $\overrightarrow{n_z}$ and $\overrightarrow{n_r}$ being respectively the normal unit vectors in the z and r directions:

$\forall (r, t)$:

$$\text{at } z = 0: \begin{cases} k_{th}\vec{\nabla}T \cdot \overrightarrow{n_z} + \frac{1}{3\kappa}\vec{\nabla}G \cdot \overrightarrow{n_z} = \gamma(r)\varphi(t) + h(T_0 - T) \\ \frac{2}{3}\vec{\nabla}G \cdot \overrightarrow{n_z} + \kappa G = 4\kappa n^2 \sigma T^4 \end{cases}$$

$$\text{at } z = H: \begin{cases} k_{th}\vec{\nabla}T \cdot \overrightarrow{n_z} + \frac{1}{3\kappa}\vec{\nabla}G \cdot \overrightarrow{n_z} = h(T_0 - T) \\ \frac{2}{3}\vec{\nabla}G \cdot \overrightarrow{n_z} + \kappa G = 4\kappa n^2 \sigma T^4 \end{cases}$$

Where $\gamma(r) = 1$ if $r \leq R_{\varphi(t)}$ and $\gamma(r) = 0$ if $r > R_{\varphi(t)}$.

$\forall(z,t)$:

$$\text{at } r = 0: \begin{cases} k_{th}\left(\vec{\nabla}T \cdot \overrightarrow{n_r}\right) + \frac{1}{3\kappa}\left(\vec{\nabla}G \cdot \overrightarrow{n_r}\right) = 0 \\ \frac{2}{3}\left(\vec{\nabla}G \cdot \overrightarrow{n_r}\right) + \kappa G = 4\kappa n^2 \sigma T^4 \end{cases}$$

$$\text{at } r = R: \begin{cases} k_{th}\left(\vec{\nabla}T \cdot \overrightarrow{n_r}\right) + \frac{1}{3\kappa}\left(\vec{\nabla}G \cdot \overrightarrow{n_r}\right) = h(T_0 - T) \\ \frac{2}{3}\left(\vec{\nabla}G \cdot \overrightarrow{n_r}\right) + \kappa G = 4\kappa n^2 \sigma T^4 \end{cases}$$

These boundary conditions correspond to equations (7) and (8).

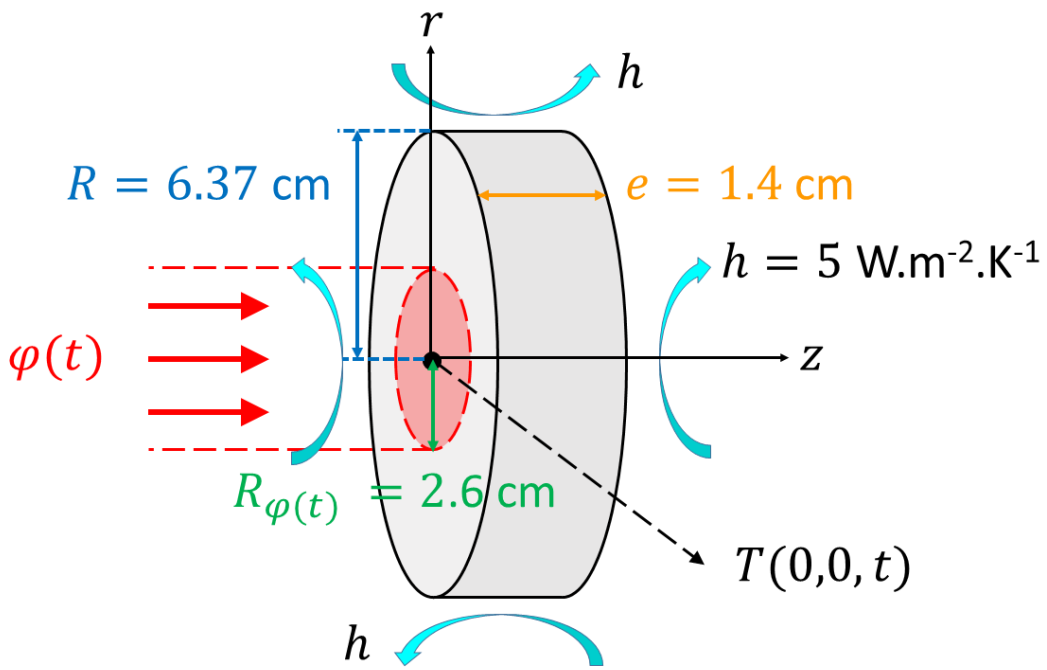


Figure 2. Sketch of the considered axisymmetric test problem

According to a previous study [17], an iterative resolution of the coupled energy conservation equation and the radiative transfer equation is implemented by using the finite volume method [20]. A second-order centered scheme is used to approximate the space derivative of both temperature and incident radiation. An implicit first-order scheme is used to approximate the time derivative of temperature. The tridiagonal equation system obtained is solved iteratively, using the Thomas algorithm [21], in two steps: (i) the conduction part is solved assuming the incident radiation known, (ii) the radiation part is solved considering the temperature field obtained at the previous step, until convergence. Validation tests for this reference model were performed and presented in [17] [18].

It is worth noticing that although the general form of the ROMs equations is independent of the geometry, ROMs are built using data simulated for a given geometric configuration. For other geometries, ROMs of similar form but with different parameter values need to be built from new data.

6.2 Identification of a series of ROMs

Instead of a Cartesian regular mesh of the (k_{th}, κ) parameter space, an Improved Hypercube Sampling (IHS) approach [22] has been used in order to cover the space with a limited number of (k_{th}, κ) couples. Using IHS the coordinates in the parameters space are regularly spaced out but the set is formed so that any two distinct (k_{th}, κ) couples do not share a common k_{th} or κ value and in such way that the parameter space is covered as uniformly as possible. Chosen ranges of parameter values are $k_{th} \in]0; 2[\ W.m^{-1}.K^{-1}$ and $\kappa \in]0; 2000[\ m^{-1}$.

The input data for the identification of a series of ROMs are the set of $N_c^{id} = 100$ couples (k_{th}, κ) depicted by red dots in Figure 3. The heat flux signal $\delta\varphi^{data}(t)$ used for the identification of the ROM constitutive parameters is shown in red in Figure 4. It is composed of a step signal of magnitude 5 $kW.m^{-2}$ during 1 s followed by a zero signal up to 2.5 s. The output data are the corresponding 100 temperature evolutions $\delta T_{obs}^{data}(t)$ at the center of the heated face ($N_{obs} = 1$), computed with the detailed model (DM). The time step used for the DM computations is $2.5 \times 10^{-5}\ s$. The heat flux signal $\delta\varphi^{data}(t)$ and the 100 temperature signals $\delta T_{obs}^{data}(t)$ are then sampled with a time step $2.5 \times 10^{-2}\ s$, so that only $N_t^{id} = 101$ instants are used for the ROMs identification.

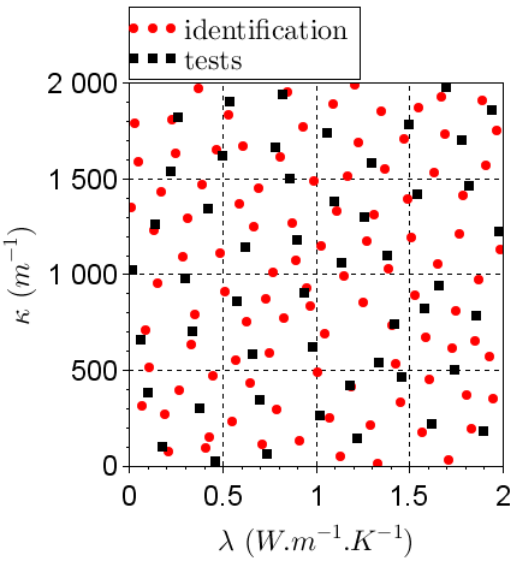


Figure 3. (k_{th}, κ) couples used for ROMs identification and validation.

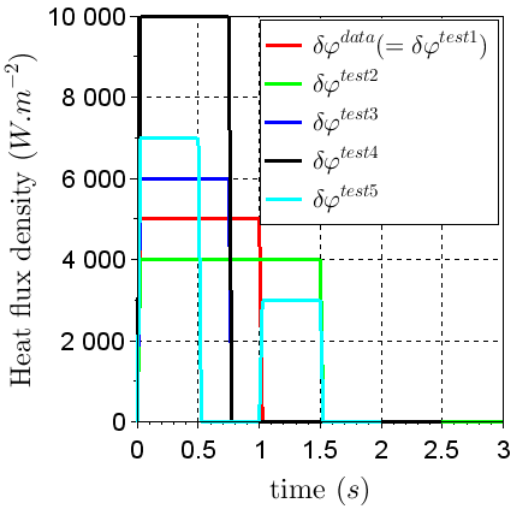


Figure 4. Heat flux densities used for ROMs identification and validation.

A series of ROMs of order m = 1 to 6 has been constructed by applying the identification procedure described in section 5.2 and using these input-output data. The value of the mean quadratic error $\sigma_{id}^{(m)}$ between DM and ROM, defined by equations (41) and (40), is shown in Figure 5 as a function of ROM order m (red curve). As expected, $\sigma_{id}^{(m)}$ decreases with the order m, down to 0.029 K for m = 6. ROMs of higher orders did not lead to further improvement.

In order to add insight to the global quantity $\sigma_{id}^{(m)}$ on all 100 (k_{th},κ) couples, the quantity $\sigma_{id,couple}^{(m)}(j), j \in [1; N_c^{id} = 100]$, related to each (k_{th},κ) couple, is defined as:

$$\sigma_{id,couple}^{(m)}(j) = \sqrt{\frac{\sum_{i=1}^{N_{obs}} \sum_{k=1}^{N_t^{id}} \left([\delta T_{obs}]_i(j,t_k,\theta,H) - [\delta T_{obs}^{data}]_i(j,t_k) \right)^2}{N_{obs} N_t^{id}}}, j \in [1; N_c^{id}]$$

Figure 6 shows values of $\sigma_{id,couple}^{(6)}$, thus corresponding to the order 6 ROM, for all 100 (k_{th},κ) couples used for ROMs identification. The lower k_{th} is, the larger the values of $\sigma_{id,couple}^{(6)}$ are. The maximum value is 0.128 K corresponding to (k_{th},κ)=(0.01,1350) and the minimum value is 0.012 K for the highest values of k_{th}. For $k_{th} \geq 0.25$ W.m^{-1}.K^{-1}, values are less than 0.037 K. The color scale is common to this figure and all similar ones in the following, the minimum and maximum values of the color scale being respectively the minimum and maximum values among all cases, i.e. identification and the five validation tests.

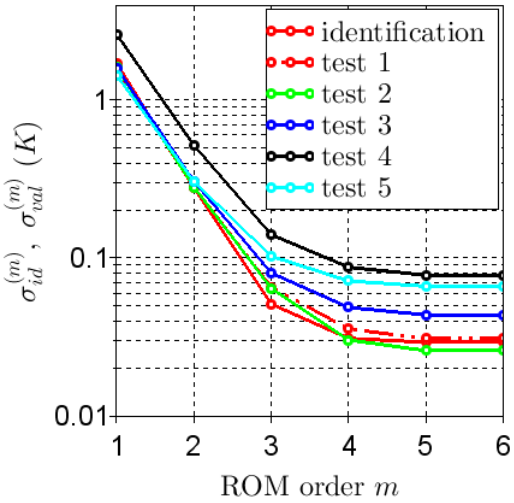


Figure 5. ROMs identification and validation tests: mean quadratic errors $\sigma_{id}^{(m)}$ and $\sigma_{val}^{(m)}$ between DM and ROM as a function of ROM order m.

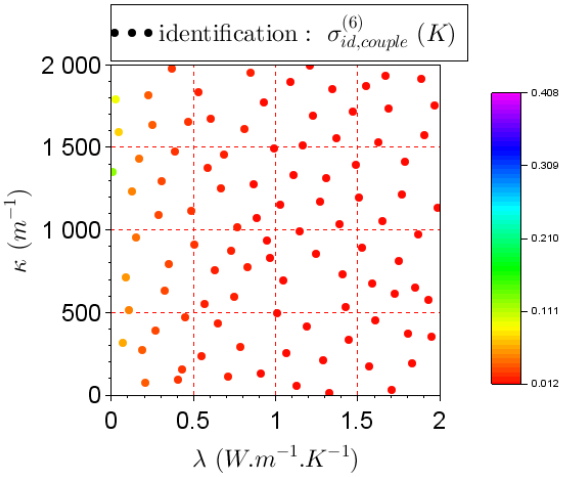


Figure 6. ROMs identification: value of $\sigma_{id,couple}^{(6)}(j), j \in [1; N_c^{id} = 100]$ for order 6 ROM.

In addition, temperature evolutions for 6 different (k_{th},κ) couples are shown in Figure 7 and Figure 8 in order to assess the ability of the order 6 ROM to reproduce the DM outputs whatever the parameters values in the considered range.

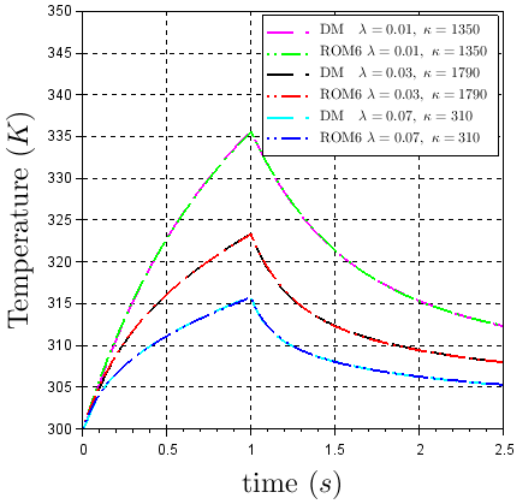


Figure 7. Identification: temperatures computed by DM and order 6 ROM for (k_{th}, κ)=(0.01,1350), (0.03,1790) and (0.07,310)

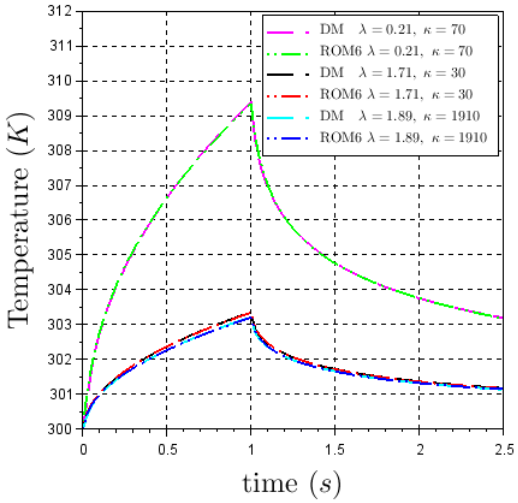


Figure 8. Identification: temperatures computed by DM and order 6 ROM for (k_{th}, κ)=(0.21,70), (1.71,30) and (1.89,1910)

6.3 Validation of the identified ROMs

Once the ROMs are identified, some test cases are conducted for the ROMs validation: a second set of N_c^{val} = 50 couples (k_{th}, κ) depicted by the black squares in Figure 3 is used as input data for the ROMs. Five different tests, hereafter referred to as test 1 to test 5, are performed, each one with a different applied heat flux density signal:

1. $\delta\varphi^{test1}(t) = \delta\varphi^{data}(t)$ used for the identification phase, shown in red in Figure 4: step signal of magnitude 5 $kW.m^{-2}$ during 1 s followed by a zero signal up to 2.5 s;
2. $\delta\varphi^{test2}(t)$ shown in green in Figure 4: step signal of magnitude 4 $kW.m^{-2}$ during 1.5 s followed by a zero signal up to 3 s;
3. $\delta\varphi^{test3}(t)$ shown in blue in Figure 4: step signal of magnitude 6 $kW.m^{-2}$ during 0.75 s followed by a zero signal up to 2 s;
4. $\delta\varphi^{test4}(t)$ shown in black in Figure 4: step signal of magnitude 10 $kW.m^{-2}$ during 0.75 s followed by a zero signal up to 2.5 s;
5. $\delta\varphi^{test5}(t)$ shown in cyan in Figure 4: step signal of magnitude 7 $kW.m^{-2}$ during 0.5 s followed by a zero signal up to 1 s, then step signal of magnitude 3 $kW.m^{-2}$ during 0.5 s followed by a zero signal up to 2 s.

The ROMs tested are exactly the ones that have been identified in section 6.2.

For each validation test, the resulting 50 temperature evolutions $\delta T_{obs}^{test}(t)$ at the center of the front face are compared with temperatures computed with the DM for the same input parameters and heat flux signal. The time sampling is the same as for data used for ROMs identification. The mean quadratic global error $\sigma_{val}^{(m)}$ between DM and ROM of order m as well

as the mean quadratic error $\sigma_{val,couple}^{(m)}(j), j \in [1; N_c^{val} = 50]$ associated to each (k_{th}, κ) couple, are defined similarly as $\sigma_{id}^{(m)}$ and $\sigma_{id,couple}^{(m)}(j), j \in [1; N_c^{id} = 100]$, respectively.

The value of $\sigma_{val}^{(m)}$ is shown in Figure 5 as a function of ROM order m for test 1 (dot-dashed red curve), test 2 (green curve), test 3 (blue curve), test 4 (black curve) and test 5 (cyan curve). As for the identification phase, $\sigma_{val}^{(m)}$ decreases with the order m.

For test 1 the heat flux signal is the same as the one used for the ROMs construction. For each one of the 6 ROMs, $\sigma_{val}^{(m)}$ for test 1 is very close to $\sigma_{id}^{(m)}$ obtained at the end of the identification phase, which shows the robustness of the ROMs as regards to the input (k_{th}, κ) values. In particular, for m = 6, $\sigma_{val}^{(6)}$ = 0.031 K for test 1. The distribution of $\sigma_{val,couple}^{(6)}$ is also very close to the one obtained in the identification phase. In particular, for the couple (k_{th}, κ) = (0.02,1020), $\sigma_{val,couple}^{(6)}$ = 0.134 K for test 1 and the minimum value is 0.012 K for the highest values of k_{th}.

Both tests 2 and 3 correspond to a heat flux signal and supplied energy different, though not significantly, from test 1. Both lead to values of $\sigma_{val}^{(m)}$ close to the ones obtained for test 1. The error for test 2 is even slightly smaller. In particular, for m = 6, $\sigma_{val}^{(6)}$ reaches 0.026 K for test 2 and 0.044 K for test 3. For the couple (k_{th}, κ) = (0.02,1020), $\sigma_{val,couple}^{(6)}$ = 0.090 K for test 2 and 0.197 K for test 3. Minimum values of $\sigma_{val,couple}^{(6)}$ are 0.012 K for test 2 and 0.015 K for test 3.

For test 4, the heat flux magnitude is twice as large as the one used for test 1 and even if the step duration is shorter, the resulting temperatures at the center of the front face are much higher compared to those reached for both identification and test 1. For instance, temperature reaches 347 K for k_{th} = 0.02 W.m^{-1}.K^{-1} and κ = 1020 m^{-1}. For a 47 K temperature increase, the validity of the linearization becomes questionable ($4\left(T_0(x)\right)^3 \delta T(x,t)$=5.08x10^9 K^4 and $6\left(T_0(x)\right)^2 \left(\delta T(x,t)\right)^2$=1.19x10^9 K^4 in the expansion of $\left(T_0(x) + \delta T(x,t)\right)^4$). Hence, not surprisingly, for the couple (k_{th}, κ) = (0.02,1020), $\sigma_{val,couple}^{(6)}$ = 0.408 K for test 4 whereas it is 0.128 K for ROM identification and 0.134 K for test 1. The minimum value of $\sigma_{val,couple}^{(6)}$ is 0.024 K. In a more general way, for all ROMs, $\sigma_{val}^{(m)}$ for test 4 is higher than $\sigma_{val}^{(m)}$ for test 1. In particular, for m = 6, $\sigma_{val}^{(m)}$ reaches 0.078 K for test 4. However, these results show the robustness of the ROMs when pushed to their limits of validity.

Test 5, which corresponds to two successive sequences, each one consisting of a step and a relaxation, exhibits similar trends: $\sigma_{val}^{(6)}$ = 0.066 K and $\sigma_{val,couple}^{(6)}$ ranges between 0.024 K and 0.287 K for the couple (k_{th}, κ) = (0.02,1020).

Figure 9 (test 4) and Figure 10 (test 5) show the values of $\sigma_{id,couple}^{(6)}$, thus corresponding to the order 6 ROM, for all 50 (k_{th}, κ) couples used for ROMs identification. Both figures show distributions similar to the one for the order 6 ROM identification (see Figure 6) but with slight differences, especially for the maximum values as mentioned above.

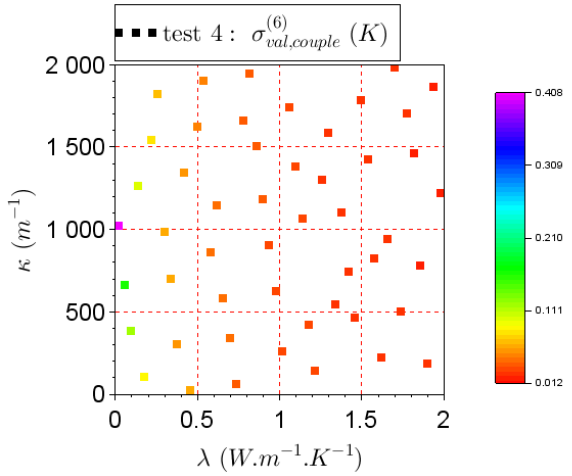


Figure 9. Validation test 4: value of $\sigma^{(6)}_{val,couple}(j), j \in [1; N_c^{id} = 50]$ *for order 6 ROM.*

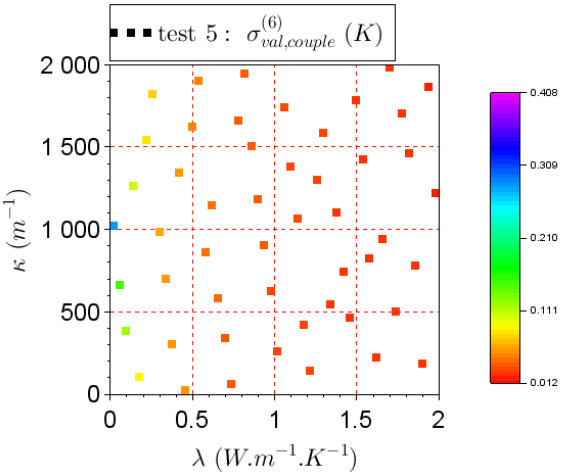


Figure 10. Validation test 5: value of $\sigma^{(6)}_{val,couple}(j), j \in [1; N_c^{id} = 50]$ *for order 6 ROM.*

In addition, temperature evolutions for 6 different (k_{th}, κ) test couples are shown for test 4 and test 5 which are the two hardest ones among the five test cases. Figure 11 and Figure 12 are relative to test 4 whereas Figure 13 and Figure 14 correspond to test 5. As for the identification phase, the order 6 ROM is able to reproduce the DM outputs for both tests regardless the parameters values in the considered range.

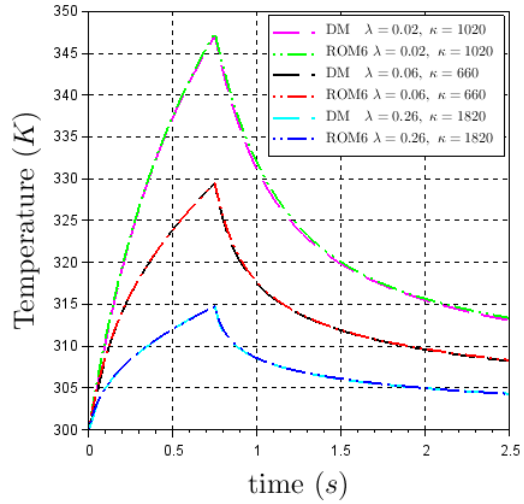


Figure 11. Validation test 4: temperatures computed by DM and order 6 ROM for (k_{th}, κ)*=(0.02,1020), (0.06,660) and (0.26,1820)*

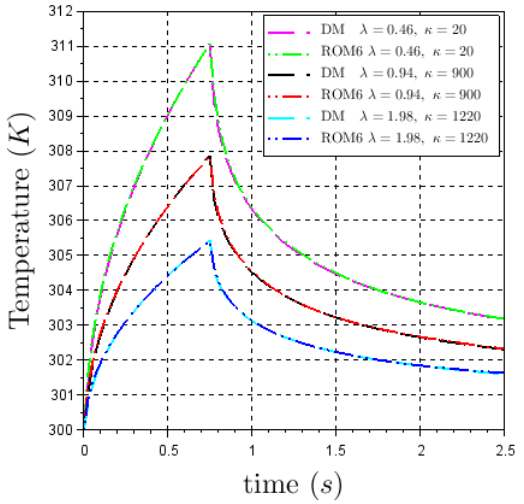


Figure 12. Validation test 4: temperatures computed by DM and order 6 ROM for (k_{th}, κ)*=(0.46,20), (0.94,900) and (1.98,1220)*

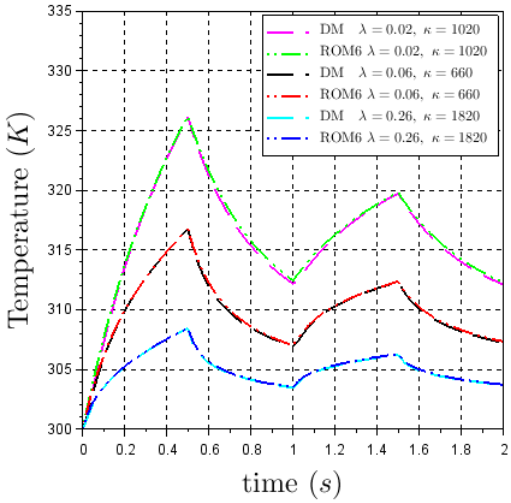


Figure 13. Validation test 5: temperatures computed by DM and order 6 ROM for (k_{th}, κ)=(0.02,1020), (0.06,660) and (0.26,1820)

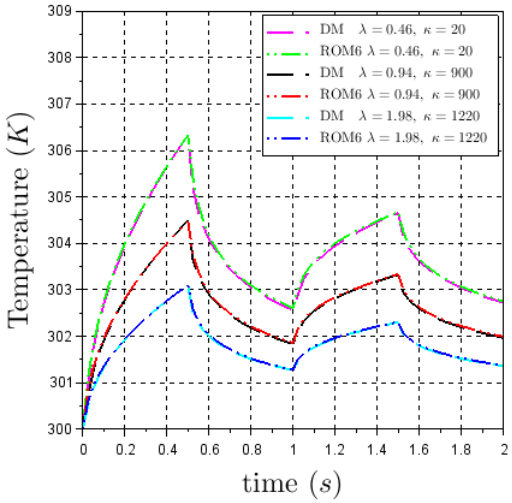


Figure 14. Validation test 5: temperatures computed by DM and order 6 ROM for (k_{th}, κ)=(0.46,20), (0.94,900) and (1.98,1220)

6.4 Computing time

Due to stability constraints, the time step for the DM is $2.5 \times 10^{-5}\ s$. With this time step, the computing time for a single simulation of 2.5 s duration is about 10^3 s with the DM on a standard PC (i5@2.3GHz, 8Go RAM). A particular form has been developed for the linear ROMs in order to ensure their stability (see section 4.3), which consequently allows using larger time steps. With a $2.5 \times 10^{-2}\ s$ time step, the computing time is only 10^{-3} s with a ROM (the size of the ROM does not make any significant difference here). At equal time steps, the ROMs thus allow a factor gain of about 10^3 compared to the DM.

7 Conclusion

In the frame of heat transfer by conduction and radiation across gray semi-transparent media for which radiative transfers can be modelled by P1 approximation, and in the context of temperature variations of limited magnitude (a few tenths of K), the construction of linear Reduced Order Models (ROMs), i.e. involving a small number of equations, by the Modal Identification Method (MIM), has been presented and performed. ROMs are explicitly parametrized by thermal conductivity k_{th} and effective absorption coefficient κ and are identified *via* the minimization of a quadratic functional based on the difference between the outputs (computed temperatures) of a reference model and those of the ROMs, for the same inputs (here a set of (k_{th}, κ) couples and an applied time-varying applied heat flux density). The approach has been applied to a test problem. This illustrative example mimics a “flash-type” experiment: a heat flux is applied on the central front part of a cylindrical sample and

the temperature at the center of the heated face is the observable quantity. The ranges of k_{th} and κ values include the values found in the literature for PMMA. The reference detailed model (DM) is a two-dimensional axisymmetric unsteady nonlinear model. First, a series of ROMs of order 1 to 6 has been built using a set of (k_{th}, κ) couples. Once identified, the ROMs have been tested with another set of couples and several applied heat flux signals different from the one used for the ROMs construction. These tests showed the ability of the ROMs to reproduce the nonlinear reference model behavior, even when pushed to their limits of validity. The accuracy of the ROM increases with the ROM order, up to order 6. Further improvement has not been noticed. In view of the very low computing times of the ROMs compared to the reference DM, they certainly can be used for solving in a fast manner an inverse problem aiming at the estimation of thermal conductivity and effective absorption coefficient, provided that sensitivities of observed temperature with respect to these parameters are large enough. Nonlinear ROMs for applications involving larger temperature variations, and thus higher radiative contributions, will be developed in future works.

Appendix

1 Galerkin projections of energy and radiative transfer equations

1.1 Galerkin projection of energy equation

Let us introduce the residue $\mathcal{R}_E(x,t)$ of energy equation (16):

$$\mathcal{R}_E(x,t) = \rho C_p \frac{\partial \delta T}{\partial t}(x,t) - \vec{\nabla}.\left(k_{th}\vec{\nabla}\delta T(x,t)\right) - \vec{\nabla}.\left(\frac{1}{3\kappa}\vec{\nabla}\delta G(x,t)\right) \qquad \text{(A.1)}$$

The Galerkin projection consists in forcing the residue $\mathcal{R}_E(x,t)$, written with approximations (22) for $\delta T(x,t)$ and (25) for $\delta G(x,t)$, to be orthogonal to each $\phi_k^{(T)}(x)$, $k \in \{1,\dots,m_T\}$, so that the projection of the residue onto the subspace of $\mathcal{L}^2(\Omega)$ generated by the $\phi_k^{(T)}$ is null. According to (23), this writes:

$$\langle \mathcal{R}_E(x,t), \phi_k^{(T)}(x)\rangle = \int_\Omega \mathcal{R}_E(x,t)\phi_k^{(T)}(x)d\Omega = 0 \qquad \forall\, k \in \{1,\dots,m_T\} \qquad \text{(A.2)}$$

Which, based on (A.1), leads to:

$$\underbrace{\int_\Omega \rho C_p \frac{\partial \delta T}{\partial t}(x,t)\phi_k^{(T)}(x)d\Omega}_{\mathcal{I}} - \underbrace{\int_\Omega \vec{\nabla}.\left(k_{th}\vec{\nabla}\delta T(x,t) + \frac{1}{3\kappa}\vec{\nabla}\delta G(x,t)\right)\phi_k^{(T)}(x)d\Omega}_{\mathcal{D}} = 0 \qquad \forall\, k \in \{1,\dots,m_T\} \qquad \text{(A.3)}$$

$\mathcal{I}$ is the inertia term and $\mathcal{D}$ gathers heat conduction and radiation fluxes in the medium.

The following steps, not detailed here, are then performed on equation (A.3):

- $\mathcal{D}$ is integrated by parts using Green formula $\int_\Omega f\vec{\nabla}.\vec{u}d\Omega = \int_\Gamma f\vec{u}.\vec{n}d\Gamma - \int_\Omega \vec{u}.\vec{\nabla}fd\Omega$;
- Thermal boundary condition (18) is introduced in the arising boundary term;
- Approximations (22) for $\delta T(x,t)$ and (25) for $\delta G(x,t)$ are injected where necessary, taking into account orthonormality of the $\phi_k^{(T)}(x),\ k \in \{1,\dots,m_T\}$ (see eq.(24)).

After taking out thermal conductivity k_{th} and effective absorption coefficient κ from integrals in order to make them appear as explicit parameters, equation (A.3) can be written as:

$$\frac{da_k^{(T)}(t)}{dt} - k_{th}\sum_{i=1}^{m_T}(M_{Td})_{ki}a_i^{(T)}(t) - \sum_{i=1}^{m_T}(M_{Th})_{ki}a_i^{(T)}(t) - \frac{1}{\kappa}\sum_{i=1}^{m_G}(M_{TG})_{ki}a_i^{(G)}(t) - V_k\delta\varphi(t) = 0 \quad \forall k \in [1;m_T] \tag{A.4}$$

Or, in matrix-vector form:

$$\frac{da^{(T)}(t)}{dt} = (k_{th}M_{Td} + M_{Th})a^{(T)}(t) + \frac{1}{\kappa}M_{TG}a^{(G)}(t) + V\delta\varphi(t) \tag{A.5}$$

Where:

$$(M_{Td})_{ki} = -\frac{1}{\rho C_p}\int_\Omega \vec{\nabla}\phi_i^{(T)}(x).\vec{\nabla}\phi_k^{(T)}(x)d\Omega \qquad \forall (k,i) \in \{1,\dots,m_T\}^2 \tag{A.6}$$

$$(M_{Th})_{ki} = -\frac{1}{\rho C_p}\int_\Gamma h(x)\phi_i^{(T)}(x)\phi_k^{(T)}(x)d\Gamma \qquad \forall (k,i) \in \{1,\dots,m_T\}^2 \tag{A.7}$$

$$(M_{TG})_{ki} = -\frac{1}{3\rho C_p}\int_\Omega \vec{\nabla}\phi_i^{(G)}(x).\vec{\nabla}\phi_k^{(T)}(x)d\Omega \qquad \forall k \in \{1,\dots,m_T\}, \forall i \in \{1,\dots,m_G\} \tag{A.8}$$

$$V_k = \frac{1}{\rho C_p}\int_\Gamma \gamma(x)\phi_k^{(T)}(x)d\Gamma \qquad \forall k \in \{1,\dots,m_T\} \tag{A.9}$$

1.2 Galerkin projection of Radiative Transfer Equation

Let us call $\mathcal{R}_R(x,t)$ the residue of linearized RTE (17). The corresponding Galerkin projection writes:

$$\langle \mathcal{R}_R(x,t), \phi_k^{(G)}(x)\rangle = \int_\Omega R_R(x,t)\phi_k^{(G)}(x)d\Omega = 0 \qquad \forall k \in \{1,\dots,m_G\} \tag{A.10}$$

Which, based on linearized RTE (17), leads to:

$$\langle R_R(x,t), \phi_k^{(G)}(x)\rangle = \underbrace{\int_\Omega \vec{\nabla}.\left(\frac{1}{3\kappa}\vec{\nabla}\delta G(x,t)\right)\phi_k^{(G)}(x)d\Omega}_{\mathcal{L}}$$
$$\underbrace{-\int_\Omega \kappa\left(\delta G(x,t) - 16n^2\sigma\left(T_0(x)\right)^3\delta T(x,t)\right)\phi_k^{(G)}(x)d\Omega}_{\mathcal{N}} = 0 \qquad \forall k \in [1; m_G] \tag{A.11}$$

The following steps, not detailed here too, are then performed on equation (A.11):

- $\mathcal{L}$ is integrated by parts using Green formula $\int_\Omega f\vec{\nabla}.\vec{u}d\Omega = \int_\Gamma f\vec{u}.\vec{n}d\Gamma - \int_\Omega \vec{u}.\vec{\nabla}fd\Omega$;
- Radiative boundary condition (19) is introduced in the arising boundary term;
- Approximations (22) for $\delta T(x,t)$ and (25) for $\delta G(x,t)$ are injected where necessary, taking into account orthonormality of the $\phi_k^{(G)}(x),\ k \in \{1, \dots, m_G\}$ (see eq.(26)).

After taking out effective absorption coefficient κ from integrals in order to make it appear as an explicit parameter, equation (A.11) can be written as:

$$\frac{1}{\kappa}\sum_{i=1}^{m_G}(M_{G0})_{ki}a_i^{(G)}(t) + \kappa a_k^{(G)}(t) + \sum_{i=1}^{m_G}(M_{G2})_{ki}a_i^{(G)}(t)$$
$$= \kappa\sum_{i=1}^{m_T}(M_{GT1})_{ki}a_i^{(T)}(t) + \sum_{i=1}^{m_T}(M_{GT2})_{ki}a_i^{(T)}(t) \qquad \forall k \in [1; m_G] \tag{A.12}$$

Or, in matrix-vector form with I_{m_G} as the identity matrix of size $m_G \times m_G$:

$$\left(\frac{1}{\kappa}M_{G0} + \kappa I_{m_G} + M_{G2}\right)a^{(G)}(t) = (\kappa M_{GT1} + M_{GT2})a^{(T)}(t) \tag{A.13}$$

Where:

$$(M_{G0})_{ki} = \frac{1}{3}\int_\Omega \vec{\nabla}\phi_i^{(G)}(x).\vec{\nabla}\phi_k^{(G)}(x)d\Omega \qquad \forall (k,i) \in [1; m_G]^2 \tag{A.14}$$

$$(M_{G2})_{ki} = \frac{1}{2}\int_\Gamma \phi_i^{(G)}(x)\phi_k^{(G)}(x)d\Gamma \qquad \forall (k,i) \in [1; m_G]^2 \tag{A.15}$$

$$(M_{GT1})_{ki} = 16\int_\Omega n^2\sigma\left(T_0(x)\right)^3\phi_i^{(T)}(x)\phi_k^{(G)}(x)d\Omega \qquad \forall k \in [1; m_G], \forall i \in [1; m_T] \tag{A.16}$$

$$(M_{GT2})_{ki} = 8\int_\Gamma n^2\sigma\left(T_0(x)\right)^3\phi_i^{(T)}(x)\phi_k^{(G)}(x)d\Gamma \qquad \forall k \in [1; m_G], \forall i \in [1; m_T] \tag{A.17}$$

2 ROMs construction: optimization algorithms

2.1 Particle Swarm Optimization (PSO) for vector θ

A Particle Swarm Optimization (PSO) algorithm [14] has been used for the estimation of vector θ. Our home-made PSO code uses a circular neighborhood of size 3. A swarm of N_p=20 particles has been used. At iteration $k+1$ of the PSO algorithm, pseudo-velocity $v_j^{p,k+1}$ and position $\theta_j^{p,k+1}$ of particle p in direction j of the unknown parameters space of dimension $N_\theta(m)$ are updated according to the following sequence:

$$v_j^{p,k+1} = \chi v_j^{p,k} + \lambda\, rand_p\left(\theta_j^{p,best} - \theta_j^{p,k}\right) + \lambda\, rand_g\left(\theta_j^{p,g} - \theta_j^{p,k}\right)$$

$$\theta_j^{p,k+1} = \theta_j^{p,k} + v_j^{p,k+1}$$

$\theta^{p,best}$ is the best position found by particle p and $\theta^{p,g}$ is the best position found by its informants, up-to-date. $rand_p$ and $rand_g$ are random numbers taken from a uniform distribution in [0:1]. Parameters χ = 0.729 and λ = 1.494 have been used. This set was previously tested in [22].

A parallelized version has been used in the present work: equation (36) (with A_G given by (35)) which corresponds to vector θ associated with each particle, is solved by a dedicated process, for all couples $(k_{th},\kappa)_j^{data}, j \in \left[1; N_c^{id}\right]$ and all instants $t_k, k \in \left[1; N_t^{id}\right]$.

At each iteration of the PSO algorithm, after each update of the particles position, a non-orthogonal matrix A_{TG}^0 is formed. A QR factorization of A_{TG}^0 is performed (using LAPACK subroutines) and A_{TG} in the ROM is set to be the orthogonal matrix Q.

2.2 Ordinary Least Squares for matrix H

At each iteration of the PSO algorithm, for each particle of the swarm, parameters in θ are fixed: the low order state vector $X^{(T)}(t) \in \mathbb{R}^m$ is computed for all couples $(k_{th},\kappa)_j^{data}, j \in \left[1; N_c^{id}\right]$ at all instants $t_k, k \in \left[1; N_t^{id}\right]$ by solving equation (36) with $\delta\varphi^{data}(t)$. The resolution of this linear system of equations involving symmetric matrices is performed using dedicated LAPACK subroutines.

Matrix $\mathbb{X} \in \mathbb{R}^{m\times(N_c^{id}N_t^{id})}$ is then formed:

$$\mathbb{X} = \left[X^{(T)}(1,t_1)\cdots X^{(T)}(1,t_{N_t^{id}})\cdots X^{(T)}(N_c^{id},t_1)\cdots X^{(T)}(N_c^{id},t_{N_t^{id}})\right]$$

Matrix $\mathbb{T}^{data} \in \mathbb{R}^{N_{obs}\times(N_c^{id}N_t^{id})}$ is formed in a similar way:

$$\mathbb{T}^{data} = \left[\delta T_{obs}^{data}(1,t_1)\cdots\delta T_{obs}^{data}(1,t_{N_t^{id}})\cdots\delta T_{obs}^{data}(N_c^{id},t_1)\cdots\delta T_{obs}^{data}(N_c^{id},t_{N_t^{id}})\right]$$

Calling $\mathbb{T}$ the corresponding matrix for the ROM, one has, according to output equation (39):

$$\mathbb{T} = H\mathbb{X} \qquad \text{(A.18)}$$

Using the Frobenius norm $\|M\|_F = \left(\sum_i\sum_j M_{ij}^2\right)^{1/2}$ of a real valued matrix M and equation (A.18), the quadratic functional $\mathcal{J}_{id}^{(m)}(\theta,H)$ defined by equation (40) can also be written:

$$\mathcal{J}_{id}^{(m)}(\theta,H) = \|\mathbb{T}-\mathbb{T}^{data}\|_F^2 = \left\|\mathbb{T}^T-\mathbb{T}^{data^T}\right\|_F^2 = \left\|\mathbb{X}^TH^T-\mathbb{T}^{data^T}\right\|_F^2$$

which also writes, using the L_2 norm $\|V\|_2 = (\sum_i V_i^2)^{1/2}$ of a real valued vector V:

$$\mathcal{J}_{id}^{(m)}(\theta,H) = \sum_{j=1}^{N_{obs}}\left\|\mathbb{X}^T(H^T)_j-\left(\mathbb{T}^{data^T}\right)_j\right\|_2^2$$

where $(H^T)_j \in \mathbb{R}^m$ and $\left(\mathbb{T}^{data^T}\right)_j \in \mathbb{R}^{N_c^{id}N_t^{id}}$ are respectively the j^{th} column of $H^T \in \mathbb{R}^{m\times N_{obs}}$ and $\mathbb{T}^{data^T} \in \mathbb{R}^{(N_c^{id}N_t^{id})\times N_{obs}}$.

So, for θ fixed, searching for H minimizing $\mathcal{J}_{id}^{(m)}(\theta,H)$ is equivalent to minimizing each one of the $\left\|\mathbb{X}^T(H^T)_j-\left(\mathbb{T}^{data^T}\right)_j\right\|_2^2$, $j\in[1;N_{obs}]$.

$\mathbb{X}^T \in \mathbb{R}^{(N_c^{id}N_t^{id})\times m}$ and $\left(\mathbb{T}^{data^T}\right)_j \in \mathbb{R}^{N_c^{id}N_t^{id}}$ are known, hence under the condition $N_c^{id}N_t^{id} \geq m$ (easily fulfilled in practice since m ranges between 1 to less than 10), the estimation of $(H^T)_j \in \mathbb{R}^m$ using Ordinary Least Squares consists in solving:

$$\mathbb{X}\mathbb{X}^T(H^T)_j = \mathbb{X}\left(\mathbb{T}^{data^T}\right)_j \qquad j\in[1;N_{obs}]$$

Matrix H^T is therefore estimated by simply solving:

$$\mathbb{X}\mathbb{X}^TH^T = \mathbb{X}\mathbb{T}^{data^T} \qquad \text{(A.19)}$$

Acknowledgements

This work was partially supported by the China Scholarship Council Foundation. The authors would also thank CPER (2015-2020) and ERDF (2014-2020) grants for supporting this work through the funding of experimental equipment.

References

[1] P. Y. Wang, H. P. Tan, L. H. Liu and J. F. Luo, "Heat transfer in translucent thermal barrier coatings of turbine engine," *Journal of Aerospace Power*, vol. 15, no. 3, pp. 268-273, 2000.

[2] P. Y. Wang, H. E. Cheng and H. P. Tan, "Transient thermal analysis for semi-transparent composite thermal barrier coatings," *Journal of Shanghai Jiao Tong University,* vol. 36, no. 2, pp. 180-184, 2002.

[3] H. M. Park, T. H. Kim and J. H. Lee, "Dynamic simulation of thermal radiation in participating media by means of mode reduction," *Journal of Quantitative Spectroscopy & Radiative Transfer,* vol. 62, pp. 141-166, 1999.

[4] H. M. Park and T. Y. Yoon, "Solution of inverse radiation problems using the Karhunen-Loève Galerkin procedure," *Journal of Quantitative Spectroscopy & Radiative Transfer,* vol. 68, pp. 489-506, 2001.

[5] H. M. Park and M. C. Sung, "Solution of a multidimensional inverse radiation problem by means of mode reduction," *International Journal for Numerical Methods in Engineering,* vol. 60, pp. 1949-1968, 2004.

[6] B. Gaume, F. Joly and O. Quéméner, "Modal reduction for a problem of heat transfer with radiation in an enclosure," *International Journal of Heat and Mass Transfer,* vol. 141, p. 779–788, 2019.

[7] L. Fagiano and R. Gati, "On the order reduction of the radiative heat transfer model for the simulation of plasma arcs in switchgear devices," *Journal of Quantitative Spectroscopy & Radiative Transfer,* vol. 169, p. 58–78, 2016.

[8] M. Girault, D. Petit and E. Videcoq, "Identification of Low-Order Models and Their Use for Solving Inverse Boundary Problems," in *Thermal Measurements and Inverse Techniques,* H. R. Orlande, O. Fudym, D. Maillet and R. M. Cotta, Eds., CRC Press, 2011, pp. 457-506.

[9] M. Girault, E. Videcoq and D. Petit, "Estimation of time-varying heat sources through inversion of a low order model built with the modal identification method from in-situ temperature measurements," *International Journal of Heat and Mass Transfer,* vol. 53, no. 1-3, pp. 206-219, 2010.

[10] M. Girault, L. Cordier and E. Videcoq, "Parametric low-order models in transient heat diffusion by MIM. Estimation of thermal conductivity in a 2D slab," *Journal of Physics: Conference Series,* vol. 395, no. 1, 2012.

[11] K. Bouderbala, H. Nouira, M. Girault and E. Videcoq, "Experimental thermal regulation of an ultra-high precision metrology system by combining Modal Identification Method

and Model Predictive Control," *Applied Thermal Engineering,* vol. 104, pp. 504-515, 2016.

[12] L. Cordier, M. Girault and D. Petit, "Reduced Order Modeling by Modal Identification Method and POD-Galerkin approach of the heated circular cylinder wake in mixed convection," *Journal of Physics: Conference Series,* vol. 395, no. 1, 2012.

[13] M. Girault, J. Launay, N. Allanic, P. Mousseau and R. Deterre, "Development of a thermal Reduced Order Model with explicit dependence on viscosity for a generalized Newtonian fluid," *Journal of Non-Newtonian Fluid Mechanics,* vol. 260, pp. 26-39, 2018.

[14] M. Clerc, Particle Swarm Optimization, New-York: Wiley-ISTE, 2013.

[15] I. Kalashnikova, B. van Bloemen Waanders, S. Arunajatesan and M. Barone, "Stabilization of projection-based reduced order models for linear time-invariant systems via optimization-based eigenvalue reassignment," *Computer Methods in Applied Mechanics and Engineering,* vol. 272, pp. 251-270, 2014.

[16] M. F. Modest, Radiative heat transfer, third edition ed., Academic press, Elsevier, 2013.

[17] Y. Liu, Y. Billaud, D. Saury and D. Lemonnier, "Simultaneous identification of thermal conductivity and absorption coefficient of a homogeneous medium," in *16th International Heat Transfer Conference*, Beijing, China, August 10-15, 2018.

[18] Y. Liu, Y. Billaud, D. Saury and D. Lemonnier, "Simultaneous identification of thermophysical properties of semitransparent media using an artificial neural network trained by a 2D axisymmetric direct model," *Numerical Heat Transfer, Part A: Applications,* vol. 77, no. 10, pp. 890-912, 2020.

[19] R. C. Eberhart and Y. Shi, "Comparing Inertia Weights and Constriction Factors in Particle Swarm Optimization," in *Proceedings of the IEEE International Congress Evolutionary Computation*, San Diego, 2000.

[20] L. H. Li and H. P. Tan, "Transient radiation and conduction in a two-dimensional participating cylinder subjected to a pulse irradiation," *Journal of Heat Transfer,* vol. 40, pp. 877-889, 2001.

[21] B. N. Datta, Numerical Linear Algebra and Applications, 2nd ed., SIAM, 2010.

[22] B. Beachkofski and R. Grandhi, "Improved distributed hypercube sampling," in *43rd AIAA ASME ASCE AHS ASC Struct. Struct. Dyn. Mater. Conf.*, 2002.